PAPER

Check for updates

α-Zirconium hydrogenophosphate as a nano-container of 2-aminobenzimidazole for the corrosion protection of zinc in NaCl medium

I. Bouali,[a] E. Rocca,*[a] D. Veys-Renaux, [iD][a] B. Rhouta [iD][b] and A. Khalil[b]

The development of a new generation of anticorrosion pigments for paints remains an important challenge to replace the usual sparingly-soluble pigments and thus avoid the dissemination of heavy metals in the environment and the formation of holes in polymer coatings. For this purpose, α-zirconium hydrogenophosphate ($Zr(HPO_4)_2 \cdot H_2O$, denoted as α-ZrP) was intercalated with the corrosion inhibitor 2-aminobenzimidazole (ABIM). Various microstructural analyses have proven the insertion of ABIM in the interlayer space by an acid–base exchange reaction and allowed us to propose a structural model for the new ABIM-ZrP pigment. The anticorrosion properties on zinc of the ABIM-ZrP, characterized by electrochemical measurements in 0.1 M NaCl, are due to the release of ABIM molecules by an ion-exchange reaction and the pH-buffer effect of α-ZrP and the amine group of ABIM. Compared to the commercial aluminium tri-phosphate (ATP) pigment, an alkyd-polymer coating loaded with the ABIM-ZrP pigment shows very interesting electrochemical behaviour by avoiding the blistering of the polymer coating and the beginning of zinc corrosion. This effect may be due to both the tortuous effect brought by the platelet shape of the pigments and the release of ABIM once the water uptake of the polymer becomes significant.

Introduction

Despite the intensive research in the field of anticorrosion pigments for organic coatings, the replacement of chromate compounds remains tricky on some metals like zinc or zinc-coated steels.[1] Actually, the chromate anions have an efficient corrosion-inhibitor activity, good transport properties in the water film on surfaces and adequate solubility in the paint film in contact with water.[2] Unfortunately, chromate compounds are carcinogenic (CMR compounds) and highly toxic for the environment.[3] Their use is almost forbidden in Europe by the REACH and wastewater regulations. Some potential and promising alternatives are proposed in the literature. They can be classified into two main families: sparingly-soluble pigments and insoluble pigments with ion-exchange properties. Phosphate-based pigments such as zinc phosphate are certainly the most largely used and studied soluble compounds. Although zinc phosphates are known to be very efficient on steels, only a few improved formulations are proposed on zinc in the literature which need to be enriched in aluminium,

calcium, molybdenum metallic ions[4] or polyphosphate anions[5] in order to adapt the solubility of the pristine zinc phosphate. These pigments have the advantage of being inexpensive and easy to produce with an adequate particle size ranging up to nanometres.[6] Nevertheless, the dissolution of soluble pigments in the organic coating involves the formation of voids or holes, which provide some transport pathways for corrosive species and limit the protective ability of coatings.[7]

To overcome this drawback, some insoluble inorganic pigments have been developed with the property of releasing corrosion-inhibitor compounds by an ion-exchange reaction with anions (OH^-, Cl^-) or cations (H^+, Na^+) in the water inside the organic coatings, without a significant volume change in the pigment particles. These pigments are based on layered insoluble solids, functionalized to form host materials with nanometre cavities or spaces containing corrosion-inhibitor compounds.

One of the most studied nanometre host materials is the layered double hydroxide (LDH) family, successfully used to provide anionic inhibitors *via* an anion exchange reaction in the paint film.[8] Silica layered compounds and clays such as smectite are also proposed to have good efficiency to release cationic inhibitors.[9,10] The driving force of the ionic exchange in these compounds is only the difference in chemical potential, mainly due to the difference in the concentration between

a Université de Lorraine, Institut Jean Lamour, Campus Artem, 2 allée André Guinier, 54011 Nancy, France. E-mail: emmanuel.rocca@univ-lorraine.fr
b Laboratoire de Matière Condensée et Nanostructures (LMCN), Faculté des Sciences et Techniques Guéliz, Université Cadi Ayyad, BP 549 Marrakech, Maroc

the inside and outside of the material. Besides, this kind of pigment can be difficult to use in practice in paint films and are often costly to synthesize.

Recently, insoluble metallic phosphates such as alpha-zirconium hydrogenophosphate denoted as α-ZrP ($Zr(HPO_4)_2 \cdot H_2O$) were considered with success as stable nanometre containers of cationic corrosion inhibitors in corrosive media or anticorrosive pigments in organic coatings.[11–13] Crystalline α-ZrP was first prepared by Clearfield and Stynes[14] and studied by several authors for its cationic exchange capacity and acid properties in the fields of catalysis, biochemistry and physics applications.[15,16–19] Inside the lamellar cavities of its crystallographic structure, the hydrogen atoms in the pendant OH groups are very labile and can be easily exchanged with various cationic entities such as metal cations or organic compounds such as organic ammonium.[20–23] In proton-exchange materials, the driving force of the ionic exchange is both the chemical potential difference and the possible acid–base reaction between the internal proton of ZrP and the external medium.[12,13]

The goal of this paper is to develop α-ZrP nanocontainers containing a cationic organic inhibitor, which can be added to an alkyd-polymer coating. This new formulation should prevent the dissemination of heavy metals such as zinc or molybdenum into the environment. For that, a new anticorrosion pigment, α-ZrP, loaded with 2-aminobenzimidazole, was prepared and characterized to determine its chemical composition and morphology. Then, the corrosion behaviour of zinc in contact with the new pigments was evaluated by electrochemical measurements in NaCl medium, in comparison with a commercial aluminium tri-phosphate pigment (ATP). Afterwards, the anticorrosion performance of α-ZrP pigments loaded in an alkyd-type organic coating was assessed by electrochemical impedance spectroscopy over a long-time immersion in an NaCl corrosive electrolyte.

Experimental

Synthesis and characterization of α-ZrP-based pigment samples

For the synthesis of $Zr(HPO_4)_2 \cdot H_2O$ (denoted α-ZrP) and its derivatives, the reagents zirconium oxychloride ($ZrOCl_2 \cdot 8H_2O$), phosphoric acid (H_3PO_4, 85 wt%), and 2-aminobenzimidazole ($C_7H_7N_3$, 97 wt%, CAS no: 934-32-7) abbreviated as ABIM along with deionized water obtained from the Dionex™ ICW-3000 Online Water Purification System were used. All reagents were supplied by Aldrich and were used as received without further purification.

α-ZrP was synthesized by refluxing 100 g L^{-1} of $ZrOCl_2 \cdot 8H_2O$ in H_3PO_4 (6 M) at 100 °C for 24 h, according to the procedure described elsewhere.[24] The dispersion of solid α-ZrP was purified by centrifugation at 4000 rpm, rinsed with deionised water several times and dried in an oven at 60 °C.

To synthesize ABIM-loaded α-ZrP, a dispersion of 5 g L^{-1} of α-ZrP was prepared and was slowly titrated by adding an aqueous solution of 2-aminobenzimidazole (0.01 M) at a rate of 17 μL min^{-1} in a controlled way by means of Metrohm Titrando apparatus. After 72 h of titration, this dispersion was centrifuged at 4000 rpm for 30 min to recover the solid, which was thereafter washed several times with deionised water to remove excess ABIM. The solid product was dried in an oven at 60 °C for 24 h. The obtained compound was designated as ABIM-ZrP.

The pigment samples were characterized by X-ray diffraction (XRD) using a Philips X'PERT instrument equipped with a copper anticathode ($\lambda_{K\alpha}$ = 0.154 nm) in the 2θ range from 2 to 40° with a scanning rate of 5° min^{-1}. Fourier transform infrared spectra were recorded in the region 4000–380 cm^{-1} with a VERTEX 70, and KBr pressed pellets (1 wt% of sample) were used under a pressure of 1000 psi. Thermogravimetric analysis was carried out in the range of 25–1000 °C using a Labsys evo-Setaram. 13.5 mg of the sample was heated at a rate of 10 °C min^{-1} under an air flow (20 ml min^{-1}) used as a carrier gas.

The observations of zinc electrode surfaces were carried out using field emission scanning electron microscopy (JEOL JSM-6400). For cross-section metallographic observations, the samples were cut using a micro-chain saw, polished to achieve a mirror-like aspect and metalized with carbon.

Electrochemical measurements

The metallic substrates used were pure zinc plates (99.7 wt%) supplied by Goodfellow, France. For electrochemical tests on the zinc surface, the zinc electrodes (2.27 cm^2) were polished successively using SiC paper of 120, 400 and up to a final 4000 grit. After rinsing with distilled water, the electrodes were cleaned with alcohol and air dried. Afterwards, they were immediately immersed in aerated 0.1 M NaCl with or without 0.3 g L^{-1} of pigments (ATP or ABIM-ZrP) or 0.3 g L^{-1} of commercial ABIM molecules to perform comparative electrochemical measurements for 24 h.

Besides, for evaluating corrosion inhibition performances of pigment-enriched organic coatings, large zinc electrodes (11.32 cm^2) were mechanically abraded successively using SiC paper of 120, 400 and 800 grit. Commercial pure alkyd paint (provided by GIEM – Morocco), a polyester resin with a long carbon chain, was used to prepare the organic coatings, without any additives on the one hand or with a dispersion of pigments on the other hand (obtained with a mechanical propeller stirrer at 800 rpm for 30 min). Then, the organic coatings were applied with an application bar of 100 μm, resulting in a dry film thickness of about 65 μm. The coated plates were dried in air for 2 days at room temperature. The electrochemical behaviour of coated zinc was assessed in 0.5 M NaCl.

The electrochemical experiments were carried out in a classical three-electrode cell in an aerated electrolyte, and the horizontal working electrode was faced to a platinum grid used as a counter electrode, while a KCl-saturated calomel electrode (SCE) was used as a reference electrode. The measurements were carried out using a Gamry Ref 600 potentiostat monitored with Gamry software. Corrosion evaluations were conducted by first measuring the corrosion potential and thereafter record-

ing the electrochemical impedance spectrum from 100 kHz to 10 mHz with a 10 mV amplitude, after 24 hours of immersion for uncoated zinc and at different immersion times for coated substrates. The EIS data were simulated using equivalent electrical circuits with ZSimpWin 3.22 software.[25]

Results and discussion

Characterization of synthesized materials

As displayed in the titration curve (Fig. 1), the functionalization of α-ZrP particles with ABIM molecules occurs in three steps relative to pH. Initially, the dispersion of α-ZrP in water induces an acidic pH around 2.5 relative to the H^+ protons of the $-PO_4$-H groups present on the external surface of the α-ZrP particles. Between 0 and 0.2 moles of ABIM per mole of α-ZrP, the ABIM molecules are necessary to neutralize these H^+ protons of the particle surface until pH = 5.2. After this rapid step 1, no change is detected in the XRXD pattern.

In the second step, a gradual increase in pH values from 5.2 to 7 is explained by the intercalation of the ABIM molecules until the total addition of 1.2 moles of ABIM per mole of α-ZrP, according to the following acid–base reaction:

$$Zr(PO_4\text{-}H)_2 + C_7H_5N_2\text{-}NH_2 \rightarrow Zr(PO_4)(NH_3\text{-}C_7H_5N_2)(PO_4\text{-}H).$$
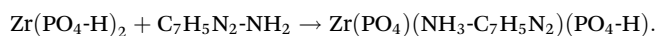
One of the labile H^+ of α-ZrP reacts with the amine group of one ABIM molecule, and the protonated ABIM is then intercalated in the lamellar space of the α-ZrP structure. The third step occurs by adding 1.2 to 2.2 moles of ABIM per mole of α-ZrP and is characterized by a slow increase in pH values from 7 to 7.4. During this last step, the intercalation of the second fraction of ABIM of α-ZrP occurs through the same type of acid–base reaction:

$$Zr(PO_4)(NH_3\text{-}C_7H_5N_2)(PO_4\text{-}H) + C_7H_5N_2\text{-}NH_2$$
$$\rightarrow Zr(PO_4)_2(NH_3\text{-}C_7H_5N_2)_2.$$

The final pH value (7.4) is reached after 3 days of titration for a ABIM/α-ZrP molar ratio of approximately 2.2. Considering the neutralization of the external H^+ by 0.2 mol of ABIM, it is confirmed that the CEC value of α-ZrP is 2, which is in accordance with the study reported by U. Costantino *et al.* on the intercalation of other heterocyclic amines.[26]

The chemical structure of α-ZrP pigments was characterized by FTIR spectroscopy as illustrated in Fig. 2. The spectrum of pristine ZrP is consistent with that reported for the α-phase.[24] The intense absorption band at around 950 to 1100 cm^{-1} corresponds to the vibrations of the PO_4 tetrahedron. The corresponding HOH bending vibration occurs at around 1600 cm^{-1}. The complex and large band structure between 3600 and 2800 cm^{-1} is attributed to the symmetric and asymmetric –OH stretching. In particular, the double peak at 3500 and 3600 cm^{-1} is mainly assigned to the PO-H vibrations.[27,28]

After the intercalation with the ABIM molecules, these two vibration bands disappear, which reveals the reaction of the O_3P-OH groups with ABIM in the interlamellar space of α-ZrP. Simultaneously, the three bands corresponding to the NH_2 vibrations (at 1450, 1550 and 1650 cm^{-1}) in the ABIM spectrum are replaced by two bands at 1500 and 1700 cm^{-1} in the ABIM-ZrP spectrum because of the modification of the conjugated π-system of the molecule.[29] This change is typically induced by amine protonation into NH_3^+ in the interlayer space. The presence of the ABIM molecule in the α-ZrP structure is also highlighted by the band at 750 cm^{-1} relative to the heterocycle vibration.[30]

The comparison of the thermogravimetric measurements of pure ABIM molecules and α-ZrP confirms the stoichiometry of intercalated compounds in Fig. 3. For the pristine α-ZrP, the mass loss at 200 °C corresponds to the loss of one molecule of

Fig. 1 Acid–base titration curve of α-ZrP compounds in suspension with ABIM solution (0.01 M) and SEM observation of ABIM-ZrP platelets.

Fig. 2 FTIR spectra of α-ZrP, ABIM-ZrP compounds and the ABIM molecule.

Fig. 3 Thermogravimetric measurements of ZrP, ABIM-ZrP compounds and the ABIM molecule.

Fig. 4 Powder XRD patterns of α-ZrP and ABIM-ZrP.

water in the interlayer space of the compound, before the final decomposition into zirconium pyrophosphate after 600 °C, as already noted in previous studies.[12,13] The thermal decomposition of ABIM occurs in two main steps between 200 °C and 600 °C. Considering that the final product of the ABIM-ZrP pigments is also ZrP_2O_7, which crystallizes in a cubic phase at 950–1000 °C, the mass loss of 8 wt% below 200 °C is clearly assigned to the loss of 2.6 mol of H_2O per mol of Zr, and the mass loss of 47 wt% between 200 and 600 °C corresponds to the decomposition of 2 mol of ABIM per mol of Zr, which is consistent with the acid–base titration results. Consequently, the chemical formula of new ABIM-ZrP pigments can be written as follows: $Zr(PO_4)_2(NH_3\text{-}C_7H_5N_2)_2$, 2.6 H_2O.

The crystallographic structure of the α-ZrP compound can be analysed with the typical powder XRD patterns displayed in Fig. 4. Pristine α-ZrP has a basal distance of 0.76 nm, and other characteristic XRD peaks at a distance for 0.44 and 0.26 nm.[14,16] Regarding ABIM-ZrP, the basal distance is moved up to 2.02 nm (corresponding to the most intense XRD peak).

Considering that the layer thickness of α-ZrP is 0.63 nm,[31] the interlayer distance in the ABIM-ZrP compound is therefore evaluated to be about 1.39 nm. According to the calculations of Chesketch software, the length and the width of the ABIM molecule are, respectively, 0.73 nm and 0.50 nm.[32] By assuming that the distance between two ABIM molecules is about 0.30 nm, a bilayer arrangement of ABIM molecules in the interlayer space is possible with a tilt angle of about 50°, as described by the scheme shown in Fig. 5. This value of tilt angle is comparable to the one reported by B. Ha *et al.* for the intercalation of hexadecylamine molecules into the interlayer space of α-ZrP.[33]

Electrochemical behaviour of zinc with α-ZrP-based pigments

Firstly, the effect of the different pigments on the electrochemical behaviour of zinc was examined by the measurements of the polarization curves and electrochemical impedance spectra in 0.1 M NaCl enriched with pigments at 0.3 g L^{-1}.

Fig. 5 (a) Representation of the ABIM molecule and (b) crystallographic model of ABIM in the interlayer region of α-ZrP.

After 24 h of immersion, the polarization curves of zinc in 0.1 M NaCl containing ATP, ABIM or ABIM-ZrP are presented in Fig. 6. These curves clearly show a decrease of the corrosion current density of zinc in the presence of ABIM (4.6×10^{-7} A cm^{-2}), ATP (3.9×10^{-6} A cm^{-2}), and ABIM-ZrP (1.8×10^{-6} A cm^{-2}) compared to the curve measured without pigments (5.4×10^{-6} A cm^{-2}). In NaCl solution, the commercial ATP pigment shows a slight inhibition effect on the anodic reaction. In con-
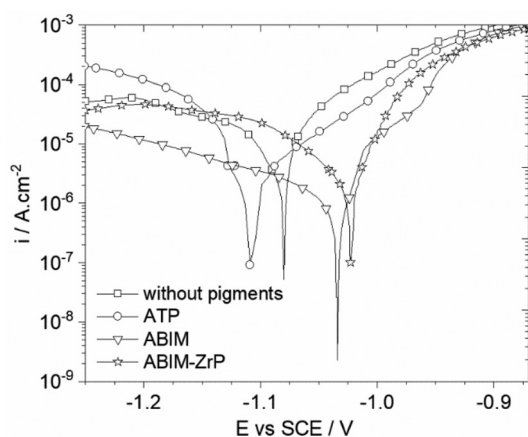
Fig. 6 Polarization curves of the zinc electrode after 24 hours of immersion in 0.1 M NaCl without or with pigments at 0.3 g L^{-1}.

trast, the presence of ABIM in NaCl solution leads to a significant decrease in cathodic current corresponding to oxygen reduction as well as the formation of a narrow anodic plateau, finally resulting in a shift of +100 mV of the corrosion potential. The same kind of corrosion inhibition effect is observed with ABIM-ZrP, to a lesser extent. Actually, the ABIM content in the ABIM-ZrP pigment is lower than in pure ABIM.

The measurement of EIS spectra after 24 hours of immersion, presented in Fig. 7, confirms and specifies the electrochemical behaviour of zinc in the presence of pigments in NaCl solution. Overall, the shape of the impedance spectra without or with pigments exhibits a single relaxation phenomenon corresponding to a capacitive loop. They can be well described using an equivalent electrical circuit composed of one (R_{CT}, CPE) time constant depicted in Fig. 7b. The electrical parameters deduced from the fit of EIS spectra are gathered in Table 1. The resistance R_e is the electrolyte resistance and the resistance R_{CT} is the charge transfer resistance at the metal/electrolyte interface. The capacitive component is described by a constant phase element (CPE), defined by the impedance: $Z_{CPE} = [Q(j\omega)^n]^{-1}$.

Actually, after 24 hours of immersion, the surface of zinc electrodes is heterogeneous, which induces a two-dimensional distribution of current and potential at the surface due to the presence of corrosion products or a passive layer. Therefore, the n factor is lower than 1 (between 0.7 and 0.9 in Table 1) which corresponds to a non-ideal capacitance. In this case, a more representative capacitance value, named effective capacitance C_{eff}, can be calculated according to the following

model:[34] $C_{eff} = \left[Q \left(\dfrac{1}{R_e} + \dfrac{1}{R_{CT}} \right)^{n-1} \right]^{\frac{1}{n}}$.

Without pigments, the charge transfer resistance of zinc remains relatively low, at around 1000 Ω cm^2, after 24 hours of immersion. Simultaneously, the capacitance is quite high, which indicates a very porous electrode, composed of many platelets of simonkolleite (Zn$_5$(OH)$_8$Cl$_2$·H$_2$O), as already
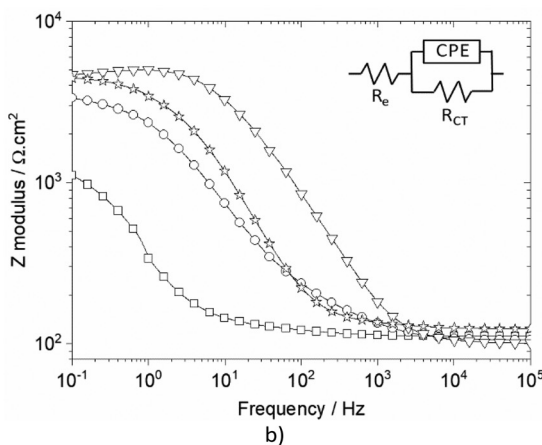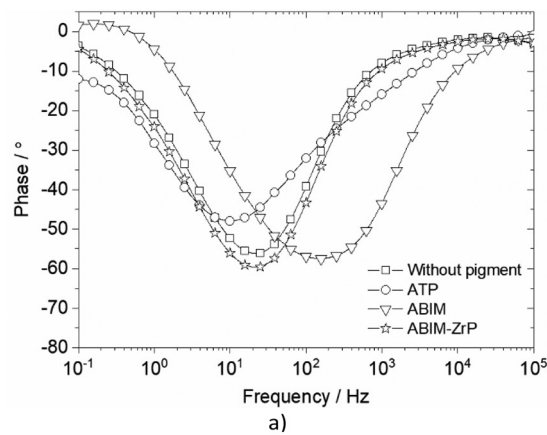

a)

b)

Fig. 7 Bode representation of impedance data of zinc in 0.1 M NaCl after 24 hours of immersion without and with 0.3 g L^{-1} of pigments: (a) Bode phase and (b) Bode modulus, with the corresponding electrical equivalent circuit used for fitting.

Table 1 Values of the equivalent electrical circuit elements calculated from the fitting results of EIS data depicted in Fig. 7

	R_e/Ω cm^2	$Q/S\ s^n$ cm^{-2}	n	R_{CT}/Ω cm^2	C_{eff}/F cm^{-2}
Without pigment	110	8.3×10^{-4}	0.77	1100	4×10^{-4}
ATP	99	8.8×10^{-5}	0.66	3500	7.4×10^{-6}
ABIM	90	3.2×10^{-6}	0.80	4500	4.0×10^{-7}
ABIM-ZrP	155	2.5×10^{-5}	0.80	4260	3.2×10^{-6}

observed in a previous study.[12] Simultaneously the high corrosion rate of zinc under these conditions is confirmed by the pH increase in the NaCl solution during the immersion (Table 2). Indeed, during the corrosion process, a significant oxygen reduction rate on zinc leads to a pH increase according to the following reaction:[35]

$$1/2 O_2 + H_2O + 2e^- \rightarrow 2OH^-.$$
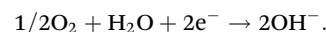
So, although the corrosion products on zinc in NaCl solution can be thick, this corrosion layer is not protective because of its significant porosity.
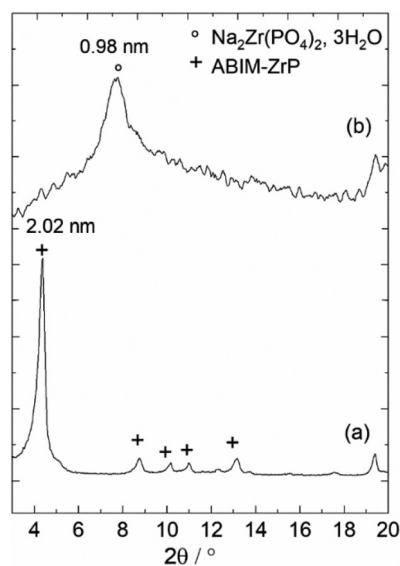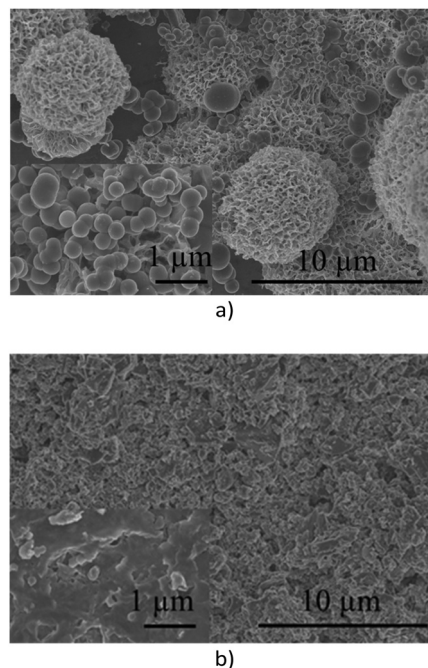
Table 2 pH evolution of 0.1 M NaCl solution (0.1 M) without and with pigment in contact with zinc

| Immersion time/h	0	3	6	9	15	24
Without pigment	6.4	6.7	7.0	7.2	7.3	7.5
ATP	6.2	6.0	6.0	6.0	6.1	6.1
ABIM	6.1	6.2	6.2	6.2	6.4	6.3
ABIM-ZrP	5.8	5.7	5.8	5.9	5.9	6.0

With ATP, the R_{CT} value increases until 3500 Ω cm^2 and the capacitance decreases, which means that the dissolution of ATP induces the formation of a denser and more protective surface layer. In the case of pure ABIM and ABIM-ZrP pigments, the R_{CT} values are about 4000 to 4500 Ω cm^2 and the capacitance values reach 1 μF cm^{-2}. Parallelly, with all pigments, the pH of the NaCl electrolyte remains approximately constant during the 24 hours of immersion (Table 2). Consequently, the kinetics of oxygen reduction on zinc is significantly reduced in the presence of ABIM and ABIM-ZrP, as observed by the measurement of polarization curves.

With ABIM-based pigments, XRD analysis of the corrosion layer at the zinc surface shows that simonkolleite remains the main corrosion product. Nevertheless, SEM observations locally reveal the presence of sphere-like particles composed of carbon and zinc, according to EDS analysis (Fig. 9a), or a change of crystallization morphology of simonkolleite on other areas (Fig. 9b).

In fact, the XRD analysis of ABIM-ZrP before and after immersion in 0.1 M NaCl in contact with zinc also reveals a shift of the characteristic diffraction peak of ABIM-ZrP (d = 2.02 nm) to attain a value of about d = 0.98 nm that corresponds to the basal distance of Na$_2$Zr(PO$_4$)$_2\cdot$3H$_2$O (Fig. 8). This

Fig. 9 Observation (SEM) of the zinc surface after 24 hours of immersion in 0.1 M NaCl with 0.3 g L^{-1} of ABIM (a) and ABIM-ZrP (b).

result indicates that ABIM ammonium was released by exchange with Na$^+$, according to the following reaction:

$$Zr(PO_4)_2(NH_3\text{-}C_7H_5N_2)_2 + 2Na^+$$
$$\rightarrow Zr(PO_4)_2Na_2 + 2C_7H_5N_2\text{-}NH_3^+.$$
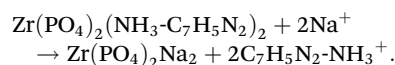
The acid–base equilibrium between the ammonium form of ABIM and its deprotonated form acts as a pH regulator on the surface (pK_a = 7 (ref. 36)), according to the following acid–base reaction:

$$C_7H_5N_2\text{-}NH_3^+ + H_2O \rightleftarrows C_7H_5N_2\text{-}NH_2 + H_3O^+.$$
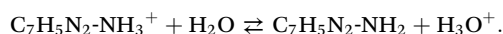
Consequently, the formation of a solid Zn^{2+}/ABIM complex is made possible in a chloride medium according to the stoichiometry proposed by H. Lopez-Sandoval *et al.*:[37]

$$Zn^{2+} + 2C_7H_5N_2\text{-}NH_2 + 2Cl^- \rightarrow Zn(C_7H_5N_2\text{-}NH_2)_2Cl_2.$$
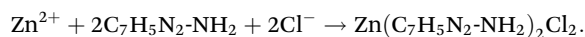
Besides, the pH buffering near the zinc surface is also provided by the presence of Zr(PO$_4$)$_2$Na$_2$ platelets, according to the equilibrium:

$$Zr(PO_4)_2Na_2 + H_3O^+ \rightleftarrows Zr(HPO_4)(PO_4)Na + Na^+ + H_2O.$$
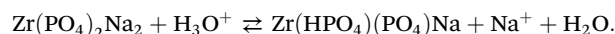
Finally, the formation of Zn^{2+}/ABIM compounds modifies the crystallization of the corrosion products, reinforces and makes denser the passivation layer, as demonstrated by the EIS analysis. This protective layer on zinc induces a significant decrease of oxygen reduction kinetics on the zinc metal and zinc oxidation kinetics, as measured in the polarization curves.

Fig. 8 Powder XRD of ABIM-ZrP pigments: (a) before and (b) after immersion in 0.1 M NaCl with 0.3 g L^{-1} of pigments in contact with zinc during 24 h.

Electrochemical behaviour of zinc coated with a paint containing α-ZrP-based inhibitors

The behaviour of zinc coated with ZrP-based pigments is further investigated in an alkyd-polymer coating during immersion in 0.5 M NaCl solution.

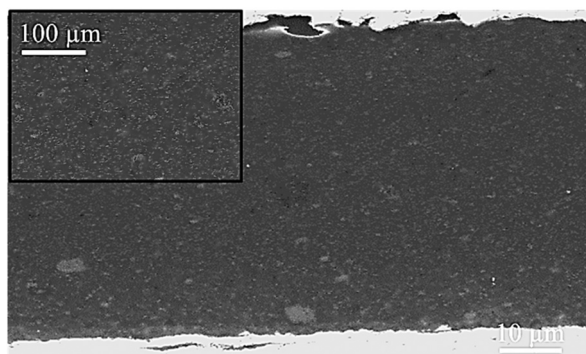Before this corrosion test, the SEM observation of a specimen cross section of zinc metal (Fig. 10) shows that the pigments are well-dispersed in the polymer film. The corrosion resistance of the coated zinc is evaluated by electrochemical impedance spectroscopy (EIS) for 32 days, and the results are displayed in Fig. 11 and 12a.

Without the pigment and with the ATP pigment, the impedance modulus at low frequency (10 mHz), corresponding to the global resistance of the interface, decreases rapidly with immersion time after 7 days, from 10^{12} to 10^5 Ω cm^2, which means that the electrolyte penetrates rapidly in the polymer film (Fig. 11 and 12). After 32 days of immersion, the impedance modulus values reach 10^4 Ω cm^2 across all the frequency ranges, which indicates blistering of the coating and the initiation of corrosion processes (Fig. 12).

With ABIM-ZrP, the impedance modulus at low frequency of the coated zinc remains very high, around 10^{12} Ω cm^2, during 15 days of immersion and decreases gradually until 10^7 Ω cm^2. It is noteworthy that the impedance modulus remains approximately 500 times higher over all the frequency ranges than the one measured with ATP or without the pigment after

Fig. 10 Metallographic cross-section observation (SEM) of alkyd resin coating loaded with the ABIM–ZrP pigment (5 wt%).
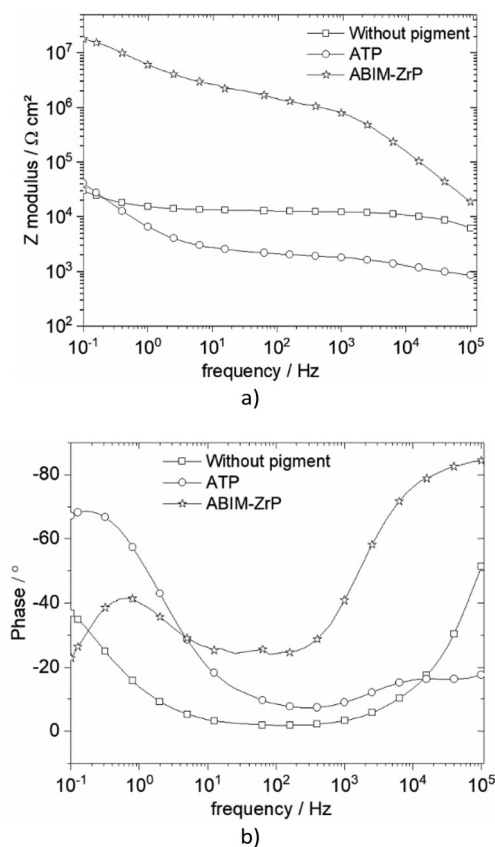

a)

b)

Fig. 11 Bode representation of impedance data of zinc coated with or without pigment-loaded alkyd resin in 0.5 M NaCl after 32 days of immersion: (a) Bode phase and (b) Bode modulus.
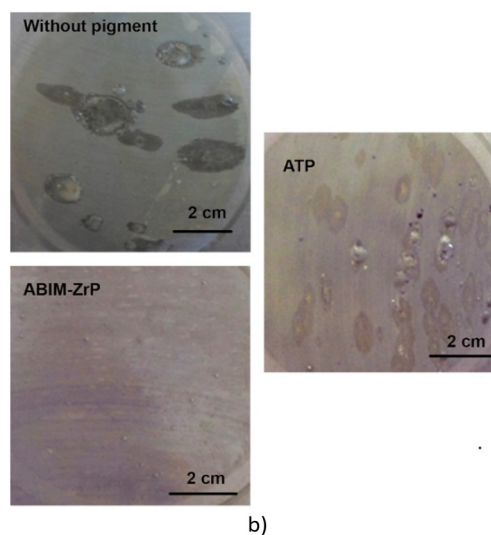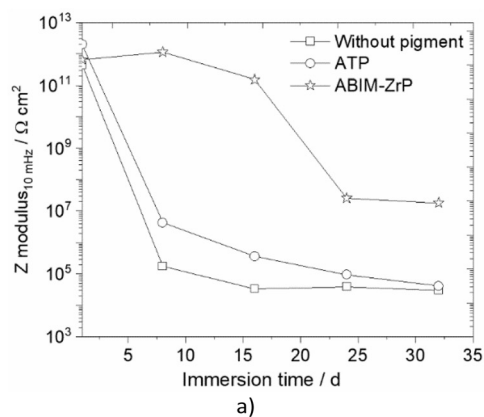

a)

b)

Fig. 12 (a) Impedance modulus at 10 mHz *versus* immersion time and (b) surface aspect after 32 days of immersion, in 0.5 M NaCl solution of zinc without or with pigment-loaded alkyd resin coating.

32 days of immersion. This high impedance value corresponds to a polymer coating without blistering and the initiation of corrosion processes, as confirmed in Fig. 12b.

This behaviour of the polymer coating loaded with ABIM-ZrP can be explained by the morphology of the ZrP-based pigments. In fact, the ZrP particles have a platelet shape and create a very efficient tortuous pathway for the electrolyte and gas in the polymer film, during the first 15 days of immersion.[38] After that, the electrolyte eventually penetrates and diffuses in the polymer film and the ABIM corrosion inhibitor is progressively released from the ZrP particles by an ionic exchange reaction with Na^+ ions. Simultaneously, ZrP and the amine function of ABIM regulate the local pH inside the polymer film to avoid the development of blistering and voluminous corrosion products.

Conclusions

Throughout this study, lamellar α-zirconium hydrogenophosphate (α-ZrP) compounds constitute very interesting alternatives to replace heavy metal-based anticorrosion pigments. α-ZrP loaded with 2-aminobenzimidazole (ABIM) corrosion inhibitors was easily synthesized by an acid–base exchange reaction. The intercalation is evidenced by the increase of the basal distance from 0.76 to 2.02 nm, indicating the insertion of 2 ABIM molecules in the interlamellar space with a tilt angle of about 50°.

In the NaCl corrosive environment, ABIM molecules are easily released by an exchange reaction with Na^+ ions to form Zn^{2+}/ABIM compounds, which modify and reinforce the corrosion product layer on zinc. Simultaneously, the α-ZrP compound and ABIM act as pH-buffers to regulate the pH on the zinc surface.

When the ABIM-ZrP particles are incorporated into an alkyd-polymer coating, their platelet shape constitutes a brick-wall structure in the polymer and forms the first efficient barrier to gases and water. When the electrolyte finally penetrates the polymer film, the release of the ABIM corrosion inhibitor ensures an efficient corrosion protection, even after 30 days of immersion in the corrosive electrolyte.

Conflicts of interest

There are no conflicts to declare.

Acknowledgements

References

1 M. Bethencourt, F. J. Botana, M. Marcos, R. M. Osuna and J. M. Sánchez-Amaya, Inhibitor properties of "green" pigments for paints, *Prog. Org. Coat.*, 2003, **46**, 280–287.

2 J. Sinko, Challenges of chromate inhibitor pigments replacement in organic coatings, *Prog. Org. Coat.*, 2001, **42**, 267–282.

3 M. Costa, Toxicity and Carcinogenicity of Cr(VI) in Animal Models and Humans, *Crit. Rev. Toxicol.*, 1997, **27**(5), 431–442.

4 V. F. Vetere, M. C. Deyá, R. Romagnoli and B. del Amo, Calcium Tripolyphosphate: An Anticorrosive Pigment for Paint, *J. Coat. Technol.*, 2001, **73**, 57–63.

5 C. Deyá, G. Blustein, B. del Amo and R. Romagnoli, Evaluation of eco-friendly anticorrosive pigments for paints in service conditions, *Prog. Org. Coat.*, 2010, **69**, 1–6.

6 N. Xie, D. Feng, H. Li, C. Gong and L. Zhen, Shape-controlled synthesis of zinc phosphatenanostructures by an aqueous solution route at room temperature, *Mater. Lett.*, 2012, **82**, 26–28.

7 A. E. Hughes, A. Trinchi, F. F. Chen, Y. S. Yang, S. Sellaiyand, J. Carr, P. D. Lee, G. E. Thompson and T. Q. Xiao, Structure and Transport in Coatings from Multiscale Computed Tomography of Coatings—New Perspectives for Electrochemical Impedance Spectroscopy Modeling, *Electrochim. Acta*, 2016, **202**, 243–252.

8 M. L. Zheludkevich, S. K. Poznyak, L. M. Rodrigues, D. Raps, T. Hack, L. F. Dick, T. Nunes and G. S. Ferreira, Active protection coatings with layered double hydroxide nanocontainers of corrosion inhibitor, *Corros. Sci.*, 2010, **52**(2), 602–611.

9 C. Zea, R. Barranco-García, J. Alcántara, B. Chico, M. Morcillo and D. de la Fuente, Hollow mesoporous silica nanoparticles loaded with phosphomolybdate as smart anticorrosive pigment, *J. Coat. Technol. Res.*, 2017, **14**, 869–878.

10 A. A. Aghzzaf, B. Rhouta, E. Rocca, A. Khalil and J. Steinmetz, Corrosion inhibition of zinc by calcium exchanged beidellite clay mineral: A new smart corrosion inhibitor, *Corros. Sci.*, 2014, **80**, 46–52.

11 T.-C. Huang, G.-H. Lai, C.-E. Li, M.-H. Tsai, P.-Y. Wan, Y.-H. Chung and M.-H. Lin, Advanced anti-corrosion coatings prepared from α-zirconium phosphate/polyurethane nanocomposites, *RSC Adv.*, 2017, **7**, 9908–9913.

12 I. Bouali, E. Rocca, D. Veys-Renaux, B. Rhouta, A. Khalil and A. Aït Aghzzaf, Ca2+-exchange in layered zirconium orthophosphate, α-ZrP: Chemical study and potential application for zinc corrosion inhibition, *Appl. Surf. Sci.*, 2017, **422**, 778–786.

13 I. Bouali, E. Rocca, D. Veys-Renaux, A. Khalil, B. Rhouta and A. Ait Aghzzaf, α-Zirconium orthophosphate as a new Zn-free anticorrosive pigment in organic coatings, *J. Solid State Electrochem.*, 2021, **25**, 831–840.

14 A. Clearfield and J. A. Stynes, The preparation of crystalline zirconium phosphate and some observations on its ion

exchange behaviour, *J. Inorg. Nucl. Chem.*, 1964, **26**, 117–129.

15 R. Vivani, G. Alberti, F. Costantino and M. Nocchetti, New advances in zirconium phosphate and phosphonate chemistry: Structural archetypes, *Microporous Mesoporous Mater.*, 2008, **107**, 58–70.

16 M. Pica, A. Donnadio, R. Vivani, E. Boccalon, M. Scattini and M. Casciola, A new challenge for nanocrystalline α-zirconium phosphate: reaction with a diepoxyalkane, *Dalton Trans.*, 2020, **49**, 3869–3876.

17 G. Alberti, M. G. Bernasconi, U. Costantino and J. S. Gill, Crystalline insoluble acid salts of tetravalent metals. XXVII. Ion exchange of trivalent cations on ionic forms of crystalline zierconium phosphate with large interlayer distances, *J. Chromatogr., A*, 1977, **132**, 477–484.

18 B. M. Mosby, A. Díaz and A. Clearfield, Surface modification of layered zirconium phosphates: a novel pathway to multifunctional materials, *Dalton Trans.*, 2014, **43**, 10328–10339.

19 E. Cruz, E. J. Broker and B. M. Mosby, Combination of intercalation and surface modification in layered zirconium phosphates: investigation of surface stability and reactivity, *Dalton Trans.*, 2020, **49**, 3841–3848.

20 A. A. Martí and J. L. Colón, Photophysical characterization of the interactions among tris(2,2′-bipyridyl)ruthenium(II) complexes ion-exchanged within zirconium phosphate, *Inorg. Chem.*, 2010, **49**, 7298–7303.

21 J. P. Gupta and D. V. Nowell, Mechanism of Some Alkylammonium-ion Exchanges by a-Zirconium Bis-(monohydrogenorthophosphate) Monohydrate, *J. Chem. Soc., Dalton Trans.*, 1979, 1178–1182.

22 R. M. Tindwa, D. K. Ellis, G.-Z. Peng and A. Clearfield, Intercalation of n-Alkylamines by a-Zirconium Phosphate, *J. Chem. Soc., Faraday Trans.*, 1985, **81**, 545–552.

23 D. M. Kaschak, S. A. Johnson, D. E. Hooks, H.-N. Kim, M. D. Ward and T. E. Mallouk, Chemistry on the edge: A microscopic analysis of the intercalation, exfoliation, edge functionalization, and monolayer surface tiling reactions of α-Zirconium phosphate, *J. Am. Chem. Soc.*, 1998, **120**, 10887–10894.

24 L. Sun, W. J. Boo, H. J. Sue and A. Clearfield, Preparation of α-zirconium phosphate nanoplatelets with wide variations in aspect ratio, *New J. Chem.*, 2007, **31**, 39–43.

25 https://www.ameteksi.com/products/software/zsimpwin.

26 U. Costantino, M. A. Massucci, A. La Ginestra, A. M. Tarola and L. Zampa, Intercalation of heterocyclic compounds in α-zirconium phosphate: Imidazole, benzimidazole, histamine and histidine, *J. Inclusion Phenom.*, 1986, **4**, 147–162.

27 M. Casciola, A. Donnadio, F. Montanari, P. Piaggio and V. Valentini, Vibrational spectra and H-bondings in anhydrous and monohydrate a-Zr phosphates, *J. Solid State Chem.*, 2007, **180**, 1198–1208.

28 G. Busca, V. Lorenzelli, P. Galli, A. La Ginestra and P. Patrono, A fourier-transform infrared and catalytic study of the evolution of the surface acidity of zirconium phosphate following heat treatment, *J. Chem. Soc., Faraday Trans. 1*, 1987, **83**, 853–864.

29 S. E. Horsley, D. V. Nowell and D. T. Stewart, The infrared and Raman spectra of α-zirconium phosphate, *Spectrochim. Acta, Part A*, 1974, **30**, 535–541.

30 B. B. Ivanova, Solid state linear dichroic infrared spectral analysis of benzimidazoles and their N1-protonated salts, *Spectrochim. Acta, Part A*, 2005, **62**, 58–65.

31 A. Clearfield and S. D. Smith, The crystal structure of zirconium phosphate and the mechanism of its ion exchange behavior, *J. Colloid Interface Sci.*, 1968, **28**(2), 325–330.

32 E. B. Sas, M. Cevik and M. Kurt, Experimental and theoretical analysis of 2-amino 1-methyl benzimidazole molecule based on DFT, *J. Mol. Struct.*, 2017, **1149**, 882–892.

33 B. Ha, K. Char and H. S. Jeon, Intercalation mechanism, and interlayer structure of hexadecylamines in the confined space of layered α-zirconium phosphates, *J. Phys. Chem. B*, 2005, **109**, 24434–24440.

34 G. Brug, A. Van Den Eden, M. Sluyters-Rehbach and J. Sluyter, Journal of Electroanalytical Chemistry and Interfacial, *Electrochemistry*, 1984, **176**, 274.

35 X. G. Zhang, *Corrosion and Electrochemistry of zinc*, Plenum press, New York, 1996.

36 G. Jerez, G. Kaufman, M. Prystai, S. Schenkeveld and K. K. Donkor, Determination of thermodynamic pKa values of benzimidazole and benzimidazole derivatives by capillary electrophoresis, *J. Sep. Sci.*, 2009, **321**, 1087–1095.

37 H. Lopez-Sandoval, M. E. Londono-Lemos, R. Garza-Velasco, I. Poblano-Melendez, P. Granada-Macias, I. Gracia-Mora and N. Barba-Behrens, Synthesis, structure and biological activities of cobalt(II) and zinc(II) coordination compounds with 2-benzimidazole derivatives, *J. Inorg. Biochem.*, 2008, **102**, 1267–1276.

38 E. L. Cussler, S. E. Hughes and W. J. Ward, R Aris Barrier membranes, *J. Membr. Sci.*, 1988, **38**, 161–174.